Highly selective catalysis at the liquid-liquid interface micro-region

Yabin Zhang
School of Chemistry and Chemical Engineering, Shanxi University, Taiyuan 030006, China
Rammile Ettelaie
Food Colloids Group, School of Food Science and Nutrition, University of Leeds, Leeds LS2 9JT, UK
Bernard P. Binks
Department of Chemistry and Biochemistry, University of Hull, Hull. HU6 7RX, UK
Hengquan Yang (hqyang@sxu.edu.cn)
School of Chemistry and Chemical Engineering, Shanxi University, Taiyuan 030006, China

Article

Keywords: Liquid-liquid, hydrogenation, Pickering emulsion, catalytic selectivity enhancement

Posted Date: July 7th, 2020

DOI: https://doi.org/10.21203/rs.3.rs-37074/v1

Abstract

Liquid-liquid interfaces in principle have the potential to regulate the selectivity of chemical reactions because of large polar gradients and highly anisotropic microenvironments, but have not yet been well exploited. Here, we present an oil-water interface-based strategy to boost catalytic selectivity, exemplified by selective hydrogenation of α,β-unsaturated aldehydes. The key to this success is the spatially controlled assembly of tubular catalyst particles at the narrow inner interfacial layer of Pickering emulsion water droplets in oil. The catalyst particles that are assembled at the inner interfacial layer of water droplets exhibit much higher selectivity to C=O hydrogenation than ones located either at the outer interfacial layer, in the interior of droplets or at the conventionally-called Pickering emulsion interface. 92.0–98.0% selectivity to the thermodynamically and kinetically unfavorable C=O hydrogenation over the C=C hydrogenation was achieved unexpectedly. The assembly strategy reported here and the unprecedented effects of interface-induced catalytic selectivity enhancement open up a liquid-liquid interface engineering route to tune reaction outcome.

Introduction

To improve catalytic selectivity is a long-standing theme for chemical synthesis[1,2]. A typical example is the selective hydrogenation of *α,β*-unsaturated aldehydes to unsaturated alcohols, obtaining important industry-relevant intermediates. This transformation is always known as a challenging reaction because the desired hydrogenation of the C=O bond is, however, thermodynamically and kinetically unfavorable over the C=C bond[3,4]. To improve the selectivity to the C=O hydrogenation, several catalysts have been developed such as organic molecule-modified metal nanoparticles[5–7], metal-supported catalysts[8–12], bimetallic catalysts[13–15] and organometallic catalysts[16]. Despite state-of-the-art progress made and cutting-edge catalysis knowledge obtained, these methods of selectivity regulation are largely limited to the tuning of electronic state and structure of catalysts.

Oil-water interfaces in principle have the potential to regulate the selectivity of chemical reactions because they feature a high polarity gradient[17], anisotropy of a few nanometers thickness[18], interfacial acidity-basicity[19] and unique interfacial microenvironments[20,21]. An early successful example is enantio-selectivity enhancement obtained through assembling amphiphilic molecular catalysts at the biphasic interface[22,23], but this strategy is not suited for reactions involving solid particle catalysts. Recently, Pickering (particle-stabilized) emulsions have been shown to be an ideal platform for the assembly of solid particle catalysts at biphasic interfaces because of the high adsorption energy of a particle at the interfaces[24–36]. Although enhanced catalysis rates have been achieved in diverse reactions compared with conventional biphasic or monophasic systems, harnessing unique properties of Pickering emulsion interfaces to tune catalytic selectivity has scarcely been reported so far, except for the case where the selectivity was improved due to the phase-selective partitioning of reactants in a biphasic system instead of the salient features of liquid-liquid interfaces[37]. The main reason for this obstacle is that the catalyst particle at the droplet interface protrudes partly into the oil phase and partly into the water phase[27,36]. As

a consequence, it is practically difficult to precisely control the reaction solely at the aqueous interfacial layer or at the oil interfacial layer. In this context, the spatially precisely controlled assembly of catalyst particles at the interfaces of Pickering emulsion droplets for selective catalysis remains a challenging task.

Herein, we demonstrate a novel strategy for regulation of the catalytic selectivity through exquisite control of the interfacial reaction within Pickering emulsions at a microscopic level. It is exemplified by selective hydrogenation of *α,β*-unsaturated aldehydes. It was found that the assembly of catalyst particles right at the inner interfacial layer of Pickering emulsion droplets gave 97.6% selectivity to C=O hydrogenation, much higher than those at the outer interfacial layer, within the interior of droplets and at the conventionally-called Pickering emulsion interfaces (which includes both outer and inner layers, namely composite interface). We attempt to clarify the origins for such an unexpected selectivity enhancement effect. This work explored here not only opens up new opportunities to tune catalytic selectivity but also provides new insights into liquid-liquid interface reactions.

Results

Preparation and characterization of emulsifiers and catalysts

To create Pickering emulsion systems, we selected titanate nanotubes (TNTs) to prepare the solid particle emulsifier. Such a choice is based on the following considerations: (i) the narrow width of the nanotubes is helpful for the control of the interfacial reaction occurring in nanoscale regions; (ii) the hollow structure can accommodate catalytic sites, *e.g.* metal nanoparticles[38]. After modification with $CH_3Si(OCH_3)_3$ (silylation of surface Ti-OH), the nanotubes were transformed to an effective particle emulsifier, named as TNTs-C. Fourier transform infrared (FT-IR) spectra (Supplementary Fig. 1) and thermogravimetric (TG) analysis (Supplementary Fig. 2) confirm the successful modification. The loading of methyl groups was determined to be 0.5 mmol g^{-1} by elemental analysis. As the transmission electron microscopy (TEM) images in Fig. 1A and Fig. 1B show, the bare TNTs and TNTs-C are both 100–400 nm in length and 4–7 nm in width, and exhibit a uniform hollow tubular structure open at both ends. The inner pore width is 6.7 nm on average, agreeing with the N_2 sorption analysis results (Supplementary Fig. 3). TNTs before modification are highly hydrophilic *per se* since the contact angle of a water drop in air is only 29° (Fig. 1G), while TNTs-C become partially hydrophobic on account of the methyl groups grafted on their surfaces (exhibiting a water contact angle of 109°, Fig. 1G). Using TNTs-C as emulsifier allowed us to formulate water-in-toluene (w/o) Pickering emulsions with droplet sizes of 50–150 μm (Fig. 1C), which was further confirmed by fluorescent dyeing of water (Fig. 1D). Ru was chosen as a catalytically active metal because it is much less expensive compared to other noble metals. Ru nanoparticles (2–3 nm) were introduced into the interior of TNTs through impregnation of $RuCl_3 \cdot 3H_2O$ followed by reduction (Supplementary Experimental Section), leading to a Ru@TNTs catalyst[39]. This catalyst is highly hydrophilic since its water contact is 30° (Fig. 1G). The TEM images (Fig. 1E and Fig. 1F) and the X-ray diffraction (XRD) patterns (Supplementary Fig. 4) reveal that Ru nanoparticles were positioned on the

inner walls of titanate nanotubes with a high dispersion. Besides the hydrophilic Ru@TNTs catalyst, we also prepared two other hydrophobic catalysts by varying the methyl loading using a similar method: partially hydrophobic catalyst Ru@TNTs-C and more hydrophobic catalyst Ru@TNTs-C^+. Their water contact angles are 106^o and 129^o, respectively (Fig. 1G).

Identification of the liquid-liquid interface impact on selectivity

Prior to investigating the hydrogenation reactions within Pickering emulsions, we examined the reactions occurring in a single toluene phase, in a single water phase and at a planar water-toluene interface (conventional biphasic system), aiming at establishing the impact of the liquid-liquid interface on the reaction outcome (Fig. 2A). To obtain good reaction activity and selectivity, tri(sodiumphenylsulfonate)phosphine (TPPTS) was added at a fixed concentration into the reaction systems (Supplementary Fig. 5). One of the roles of TPPTS is to server as water-soluble ligand modifying the Ru nanoparticle surface to improve the conversion and selectivity. Such a surface modification was confirmed by X-ray photoelectron spectroscopy in Supplementary Fig. 6 and solid-state ^{31}P MAS NMR spectra in Supplementary Fig. 7. Ru@TNTs with the aid of TPPTS proved a good catalyst for cinnamaldehyde (CAL) hydrogenation since the CAL conversion and the selectivity to cinnamyl alcohol (COL, desired product) are much better than a Ru/SiO_2 catalyst or a Ru/TiO_2 catalyst (using commercial TiO_2 particles as support, Supplementary Fig. 5). It was notable that the methyl modification of the TNTs itself had a negligible effect on the catalytic performance since Ru@TNTs, Ru@TNTs-C and Ru@TNTs-C^+ are completely comparable in terms of selectivity and activity in a water-ethanol system (Supplementary Table 1). Under the same conditions, the single toluene system gave 42.1% conversion of CAL and 2.1% selectivity to COL, whereas the conversion and selectivity in the single water system were dramatically increased up to 69.0% and 71.5%, respectively (Fig. 2B). Interestingly, in the water-toluene biphasic system, the conversion and selectivity were improved up to 72.4% and 82.2%. For another substrate *trans*-2-hexenal, these three systems also exhibited very different reaction outcomes (Fig. 2C). The selectivity to C=O obtained in the biphasic system was much higher than that obtained in the single water phase or single toluene phase. Moreover, this hydrogenation in the biphasic system gave much higher selectivity than those in other common organic solvents (Supplementary Table 2). These results highlight an oil-water interfacial effect that impacts the catalytic selectivity. It was previously found that “on water” effects[40–42] and H-shuttle effects caused by the presence of water were reported to improve the reaction rate or alter the reaction selectivity[43–47]. However, in our case, the selectivity enhancement should not be attributed to the effects arising from the presence of water molecules since the oil-water biphasic system gave much higher selectivity than the single water system (82.2% *vs* 65.0%). The presence of a liquid-liquid interface (biphasic system) should be responsible for the catalytic selectivity enhancement (Fig. 2A, c).

Control of reaction locus at Pickering emulsion interfaces

Encouraged by the impact of the planar liquid-liquid interface on the selectivity, we transformed the above biphasic system to a Pickering emulsion system, in order to significantly increase the reaction interfacial

area through generating numerous droplets. Pickering emulsion reaction systems (w/o) were achieved using shear in the presence of Ru@TNTs-C as both emulsifier and catalyst. The assembly of Ru@TNTs-C particles at water droplet interfaces was evidenced by a fluorescent circle in 3D confocal fluorescence microscopy with FITC-I-labelled Ru@TNTs-C (Fig. 3A). For this Pickering emulsion system, the conversion (87.6%) is higher than that obtained in the biphasic system, but the selectivity decreases down to 69.6% (Fig. 4A, a). The improved conversion is due to the location of the Ru@TNTs-C catalyst particles at droplet interfaces, which promotes sufficient contact of the reactant with the catalyst. Such remarkable differences in selectivity caused by the catalyst location prompts us to further consider the interfacial reaction locus at a more microscopic level. In the Pickering emulsion system, the tubular emulsifier particles adopt an orientation parallel to the interface (Supplementary Fig. 8)[48,49]; one side of Ru@TNTs-C protrudes into the water droplet and the other side into the oil phase. These two sides, in fact, make different contributions to the observed reaction outcome because the single aqueous system and the single oil system are very different in selectivity, as revealed above. The spatially precise control of the interfacial reaction locus on a microscale and thereby discriminating the composite interfacial reaction (conventionally-called Pickering emulsion interface), the outer interfacial layer reaction, the inner interfacial layer reaction and the reaction within droplet interiors, is necessary and significant.

Although Janus particles that consist of a hydrophobic part and a hydrophilic part were successfully synthesized and can be assembled at Pickering emulsion interfaces[24,50–53], it is still difficult to control reaction locus on a microscale because it is very challenging to position catalytic sites selectively on one of the parts with nanometer sizes[50]. Fortunately, we unexpectedly found that the unique interaction between TNTs and TPPTS makes possible the spatially controlled assembly of TNTs at the droplet interface (Supplementary Fig. 9). This interaction (to be discussed later) is another role of TPPTS besides the modification of Ru nanoparticles. The use of TNTs-C as emulsifier and Ru@TNTs-C^+ as catalyst enabled us to position Ru@TNT-C^+ exclusively at the outer interfacial layer. The location of FITC-I-labelled Ru@TNT-C^+ at the outer interfacial layer of water droplets was confirmed by the presence of a fluorescent circle whose intensity gradually increases on approaching the interface from outside (Fig. 3B). This is because the Ru@TNTs-C^+ particles *per se* are too hydrophobic to assemble at droplet interfaces (Supplementary Fig. 10a), being initially distributed in the oil phase, and then spontaneously migrate to the droplet interface due to the weak interactions with the TNTs-C emulsifier in low dielectric toluene (hydrophobic interactions of particles with high aspect ratio[48,49]), as shown in Supplementary Fig. 11. Conversely, when the Ru@TNTs-C^+ catalyst was replaced with the hydrophilic Ru@TNTs catalyst (FITC-I-labelled), the catalyst assembled at the inner interfacial layer of water droplets since the intensity of the observed fluorescent circle in Fig. 3C decreases from the interface to the droplet center (the Ru@TNTs particles *per se* are too hydrophilic to assemble at droplet interfaces as revealed in Supplementary Fig. 10b; the migration of Ru@TNTs to the inner interface of water droplets was monitored by fluorescence microscopy as shown in Supplementary Fig. 12). Finally, when using partially hydrophobic silica particles SiO_2-C as emulsifier (Supplementary Experimental Section), the Ru@TNTs particles (FITC-I-labelled) were

distributed throughout the interior of the water droplets due to the absence of interactions with the emulsifier at the interfaces, confirmed by a convex fluorescence image (Fig. 3D).

Impressively, these different scenarios led to substantial differences in reaction outcome. In the CAL hydrogenation, the outer interfacial layer reaction gave 39.0% conversion and 45.2% selectivity to COL (Fig. 4A, b), both much lower than those obtained in the case of the composite interfacial reaction (Fig. 4A, a). Such low conversion and selectivity are due to the difficulty for catalyst particles at the outer interfacial layer to access water-soluble TPPTS. To our delight, the inner interfacial layer reaction gave 97.3% conversion and 97.6% selectivity (Fig. 4A, c). Such a high selectivity outperforms that obtained in most reported catalysts, even including expensive Pt catalysts (Supplementary Table 3). However, when the reaction occurred within the droplet interior (Fig. 4A, d), the CAL conversion and COL selectivity sharply dropped to 88.9% and 80.4%, respectively. For this case, the decrease in conversion can be explained by the fact that the distribution of catalyst within droplet interiors decreases the accessibility to the oil-soluble CAL in comparison to the inner interfacial layer reaction. The lowered selectivity results from the further hydrogenation due partially to the untimely transfer of COL outside the droplets. The data in Supplementary Table 4 are in support of this inference since COL was further hydrogenated to hydrocinnamyl alcohol (HCOL, 16.1%) in this case, while only 1.8% HCOL was observed in the inner interfacial layer reaction system. This inference is further supported by the experiment in which the selectivity declined on prolonging the reaction time (Supplementary Fig. 13). Moreover, the remarkable enhancements of reaction efficiency and selectivity for the inner interfacial reaction have been observed in the selective hydrogenation of other unsaturated aldehydes, for example *trans*-2-hexenal, 3-methyl-2-butenal and *cis*-4-heptenal (Fig. 4B, Fig. 4C and Fig. 4D). For all these investigated substrates, the selectivity to C=O hydrogenation is as high as 93.3–99.6%. Such an excellent selectivity is not attainable for the reported single phase systems[4,9]. Based on these results, we can conclude that the difference in selectivity is caused by changes in the reaction locus, and the assembly of catalyst particles exclusively at the inner interfacial layer significantly boosts the selectivity (the possibility of the influence of droplet surface coverage is excluded, as displayed in Supplementary Fig. 14).

Reasons for selectivity enhancement

With such interesting results, we become aware of the unique mechanism of the formation of the inner interfacial layer for highly selective catalysis. The process of the assembly of Ru@TNTs at the inner interfacial layer was tracked by fluorescence labelling (Supplementary Fig. 12). The FITC-I-labelled Ru@TNTs were dispersed in water, and the TNTs-C emulsifier particles were dispersed in toluene. Immediately after emulsification of a mixture of these two suspensions, the fluorescence intensity at the inner droplet interface gradually increased and then levelled off, while the fluorescence intensity of the interior of a droplet gradually decreased and levelled off after 10 min. This indicates that Ru@TNTs migrated from the interior of a droplet to the inner interface. The driving force for such an assembly was found to be related to the presence of TPPTS since the migration of Ru@TNTs towards the interface was not observed when TPPTS was absent (Supplementary Fig. 9). The FT-IR spectrum results reveal that TPPTS tends to adsorb onto TNTs because the $-SO_3^-$ groups in TPPTS are coordinated with surface 4-

coordinated Ti (Supplementary Fig. 15; Despite the methyl modification, the surface coordination interactions between uncovered Ti sites and -SO_3^- groups still exists)[54]. Owing to the interactions, TPPTS bearing three -SO_3^- groups can bridge the TNTs-C emulsifier and the Ru@TNTs catalyst (Fig. 3C, the other role of TPPTS), thus forming an inner interfacial layer. This inference is also supported by the following experiments. Ligands containing two -SO_3^- groups, such as disodium piperazine-1,4-diethanesulphonate and disodium butane-1,4-disulfonate, exhibited an effect similar to TPPTS but sodium allylsulfonate and sodium benzenesulfonate containing only one sulfonate group did not (Supplementary Fig. 16). These experiments confirm that the additive containing two or more -SO_3^- groups is necessary for the assembly of catalyst particles at the inner interfacial layer.

Dynamic interfacial tension measurements further support the interactions between Ru@TNTs and TNTs-C in the presence of TPPTS (Fig. 5B). The equilibrium toluene-water interfacial tension in the presence of TPPTS was measured to be 28.9 mN m^{-1}. The interfacial tension decreased to 25.0 mN m^{-1} after adding TNTs-C particles, due to the adsorption of nanoparticles[55]. Notably, when TNTs particles were introduced into the above system, the interfacial tension further declined to 15.5 mN m^{-1}, reflecting the adsorption of TNTs onto the interface due to the interaction with the TNTs-C. In contrast, if TNTs-C particles are replaced with the interface-active SiO_2-C particles, the interfacial tension does not significantly decrease after adding TNTs (23.8 mN m^{-1}, Supplementary Fig. 17), indicating the migration of TNTs to the interface did not occur (the SiO_2-C surface lacks the coordination interaction with TPPTS). These findings are consistent with the aforementioned fluorescence observations.

Based on the supportive results, we propose a mechanism for the inner interfacial reaction with high selectivity. Prior to the investigation of the interface role, we compared the Ru@TNTs catalyst with the Ru/TNTs catalyst on which Ru nanoparticles are located on outside of the titanate nanotube (Supplementary Fig. 18). The comparative results reveal that the different Ru nanoparticle location had similar reaction outcome, ruling out the possibility of the impact of the nanotube confinement space on the selectivity. The oil-soluble CAL can relatively easily contact the catalyst assembled at the inner interfacial layer, where TPPTS is enriched (supported by the results of interfacial tension in Fig. 5B)[56,57]. The resultant unique local microenvironment led to high catalytic activity. This inference is supported by the finding that the conversion is gradually increased upon increasing the TPPTS concentration in a water-toluene biphasic system (Supplementary Fig. 19). Meanwhile, as Fig. 5A illustrates, the polarity gradient at the narrow inner interfacial layer favors the hydrophilic nature of the C=O bond to access to the metal surface over the less hydrophilic C=C bond[58]. As a consequence of this inner interfacial layer-induced orientation of reactant molecules, the C=C bond hydrogenation is suppressed, while selective hydrogenation of the C=O bond is enhanced significantly. Moreover, the basicity of water droplet interfaces (due to enriching of OH^-) that was reported in literature[59,60], may also play a part in improving the selectivity since the CAL hydrogenation carried out at different pHs showed that the COL selectivity increased from 71.5% to 81.8% when the pH increased from 7 to 11 in a single water system (Supplementary Fig. 20). Additionally, the high selectivity is also related to the timely and instant removal

of COL from the inner interfacial layer to the outside of droplets, due to the shorter diffusion distance compared to the case where the reaction occurs in the droplet interior. Further hydrogenation of the C=C bond was accordingly avoided. This is in agreement with the findings that the COL selectivity decreased as reaction time was prolonged in both an aqueous system and a water-toluene biphasic system, while the HCOL selectivity increased upon prolonging the reaction time (Supplementary Fig. 13). Taken together, the impact of liquid-liquid interfaces on the selectivity is evident, although it is related to multiple factors including the polarity gradient, basicity and mass transport on the interfaces. To further confirm the liquid-liquid interface effect, we replaced TPPTS with disodium butane-1,4-disulfonate that can bridge TNTs-C and Ru@TNTs but cannot modify Ru nanoparticles because of the absence of phosphine ligand. It was found that the COL selectivity was also improved at the inner interfacial layer in comparison to the case of droplet interior reaction where disodium butane-1,4-disulfonate was not added (notably, disodium butane-1,4-disulfonate itself has no effect on the selectivity and CAL conversion, as revealed by supplementary Table 5).

To further investigate the effects stemming from the inner interfacial layer, we studied the influence of average droplet size, thickness of inner interfacial layer as well as TPPTS dosage. The reaction systems with different droplet sizes were achieved by varying the stirring rate during emulsification. Upon decreasing the droplet diameter from 300 μm to 214 μm and further to 102 μm (Supplementary Fig. 21), the CAL conversion increased gradually from 42.9% to 57.1% and then to 61.5%, and the COL selectivity increased from 88.9% to 92.7% and then to 96.8% (Fig. 5C). These increases in conversion and selectivity are caused by the increase in the total area of inner interface that manifests the inner interfacial effects. Moreover, by adding different amounts of catalytically inactive TNTs together with a fixed amount of the Ru@TNTs catalyst, we could change the thickness of the inner interfacial layer, as depicted in Fig. 5D. It was found that the CAL conversion and COL selectivity both decreased with increasing the thickness of the inner interfacial layer. This finding suggests that narrowing of the inner interfacial layer is crucial to obtaining high selectivity and conversion. This is probably because the inner interfacial layer closer to the liquid-liquid interface has a greater polarity gradient which favors access of the C=O bond to the Ru surface over the C=C bond. Additionally, we compared the inner interfacial reaction with the conventional biphasic reaction in terms of dosage of TPPTS. There is only a small decrease in selectivity (from 97.6% to 94.0%) upon decreasing the dosage of TPPTS for the inner interfacial reaction (Supplementary Fig. 22), whereas a substantial decrease in COL selectivity was observed in the conventional biphasic system (from 82.2% to 65.3%). The negligibly small decrease in COL selectivity is attributed to the inner interfacial effect that is in favor of enriching TPPTS. The findings from these three aspects further highlight the uniqueness and importance of the inner interfacial reaction.

Substrate scope and recyclability

The substrate scope was further extended to other unsaturated aldehydes beyond those in Fig. 4. As summarized in Table 1, for all the investigated substrates including various phenyl and furyl-containing unsaturated aldehydes, the inner interfacial layer reaction gave conversion of 92.4–99.3% and selectivity of 91.6–98.3%, which are all higher than those obtained in the composite interfaces of Pickering

emulsions (data in parentheses as benchmark). These results further confirm that our liquid-liquid interface strategy is generally more effective at improving the catalytic selectivity.

Another advantage of our system is the good recyclability of the catalyst (Supplementary Fig. 23a). After the first run, the Pickering emulsion was demulsified *via* centrifugation. The upper layer of toluene containing product was collected by liquid transfer, and the lower aqueous layer containing catalysts and TPPTS was used directly for the second reaction cycle. After adding fresh reactant and toluene followed by emulsification, a w/o Pickering emulsion reaction system was obtained again. In the fourth reaction cycle, the conversion and selectivity reached 91.3% and 91.8%, respectively. This slight decrease was caused by the loss of emulsifier and catalyst during multiple cycles. The loss of emulsifier led to an increase in droplet size, weakening inner interface effects (Supplementary Fig. 23b).

Discussion

We have successfully demonstrated a strategy of liquid-liquid interface to improve catalytic selectivity for the hydrogenation of unsaturated aldehydes. The key to this success is the precise assembly of tubular catalyst particles at the inner interface of w/o Pickering emulsion droplets. It is found that for all investigated *α,β*-unsaturated aldehydes the selectivity and catalysis efficiency for the inner interfacial layer reaction are much higher than those obtained for all of the composite interface reaction within Pickering emulsions, the outer interfacial layer reaction within Pickering emulsions, the reaction within droplet interiors and reactions in single aqueous or organic phases. 92.0 − 98.0% selectivity to the thermodynamically and kinetically unfavorable C = O hydrogenation over C = C hydrogenation was achieved unexpectedly. The significant enhancement in catalytic selectivity is attributed to the unique microenvironment of the inner interfacial layer of water droplets and the timely departure of unsaturated alcohol from the water droplet avoiding further hydrogenation. We envisage that the strategy of spatially precisely controlled assembly of catalysts in liquid-liquid interfaces together with the thus-obtained insights of catalytic selectivity enhancement opens up a new way to tune catalytic reactions.

Methods

Preparation of TNTs-C and TNTs-C^+

Titanate nanotubes (TNTs) were obtained by an alkaline hydrothermal treatment of TiO_2, as described by Kasuga[61]. Typically, 3.0 g anatase was dispersed in NaOH solution (120 mL, 10 mol L^{-1}) and placed in a stainless steel autoclave at 150 ^oC for 24 h. The precipitate was washed with HCl solution (0.1 M) and deionized water until pH < 8. This was then dried in an air circulating oven at 80 ^oC for 5 h, thus yielding TNTs. An amount of 1.0 g “as-synthesized” TNTs was dispersed into toluene (6 mL). A mixture of 5 mmol $CH_3Si(OCH_3)_3$ and 5 mmol $(C_2H_5)_3N$ were added into this toluene suspension. After refluxing at 120 ^oC for 6 h under a N_2 atmosphere, the obtained material was isolated through centrifugation. The sample was washed five times with toluene and then dried under air. The resultant methyl-functionalized TNTs

are denoted as TNTs-C. For TNTs-C^+, 10 mmol $CH_3Si(OCH_3)_3$ and 10 mmol $(C_2H_5)_3N$ were used. Other procedures are the same as those for TNTs-C.

General procedure for preparing Pickering emulsion reaction systems

Typically, 2.5 mL deionized water and 2.5 mL toluene were added into a 10 mL vessel containing 0.03 g TPPTS, a certain amount of the emulsifier and the catalyst (if needed). For the inner interfacial layer reaction, 0.05 g Ru@TNTs as catalyst and 0.05 g TNTs-C as emulsifier; for the droplet interior reaction, 0.05 g Ru@TNTs as catalyst and 0.05 g SiO_2-C as emulsifier; for the composite interfacial reaction, 0.05 g Ru@TNTs-C as both catalyst and emulsifier; for the outer interfacial layer reaction, 0.05 g Ru@TNTs-C^+ as catalyst (added after forming Pickering emulsion) and 0.05 g TNTs-C as emulsifier. After vigorously stirring (10,000 rpm) with a homogenizer for 2 min, w/o Pickering emulsions were obtained. Then, 1.0 mmol substrate was added for reaction into the continuous oil phase.

Hydrogenation in w/o Pickering emulsion systems

The above Pickering emulsion reaction mixture was loaded in a vessel (10 mL), and the vessel was placed in a 100 mL autoclave. Before the reaction, the autoclave was sealed and flushed with H_2 three times in order to remove any air. Afterwards the autoclave was charged with H_2 at a pressure of 3.0 MPa at room temperature. The sample was heated to 60 ^oC within 20 min and was kept at this temperature while being stirred (700 rpm). Following the reaction, the autoclave was cooled to room temperature. The products were isolated through centrifuging and then analyzed by gas chromatography (Agilent 7890A). This was equipped with a HP-5 capillary column. The resulting structures were confirmed by GC-MS (Agilent 7890B GC/5977A MS, HP-5 column). After each run, the organic phase was separated from the reaction system also by centrifuging, where the solid catalyst and emulsifier remained in the aqueous phase. In the next reaction cycle, 2.5 mL of fresh toluene and a given amount of substrate were added into the above system. All the other procedures are the same as those already described for the first reaction.

Table

Table 1 | Selective hydrogenation of different unsaturated aldehydes within different w/o Pickering emulsion systems.[a]

Entry	Substrate	Product	Conversion (%)	Selectivity (%)
1[b]	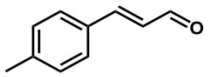	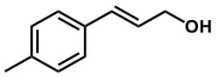	**97.0** (63.0)	**91.6** (84.6)
2[b]	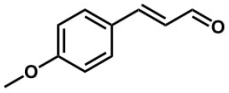	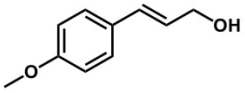	**99.0** (59.0)	**95.4** (73.0)
3	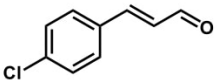	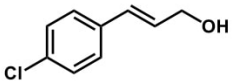	**99.3** (46.5)	**95.0** (89.2)
4	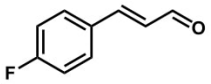	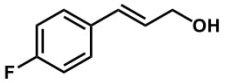	**96.4** (60.5)	**97.5** (79.6)
5	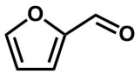	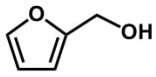	**97.0** (60.2)	**98.3** (87.1)
6	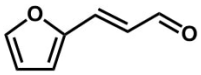	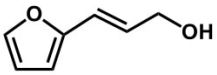	**92.4** (56.0)	**95.0** (88.5)

[a]Numbers in brackets refer to the results obtained in the composite interface reaction within the conventional Pickering emulsions. Reaction conditions: 1.0 mmol unsaturated aldehydes, 2.5 mL toluene, 2.5 mL water, 0.05 g catalyst, 0.05 g emulsifier, 0.03 g TPPTS, 60 ^{o}C, 3.0 MPa H_2, 700 rpm, 4 h. [b]4.0 MPa H_2, 6 h.

Declarations

Data availability

The data that support the plots within this paper and other findings of this study are available from the corresponding author upon reasonable request.

Competing financial interests

The authors declare no competing financial interests.

Author contributions

Q. H. Yang conceived and supervised the project; Y. B. Zhang executed the experiments and collected the data; R. Ettelaie and B. P. Binks made contributions in discussing and analyzing the experimental results.

Acknowledgements

This work was supported by the Natural Science Foundation of China (21733009, 21925203). BPB acknowledges funding from the H2020-FETOPEN-2016-2017 program of the European Commission (grant agreement no. 737266-ONE FLOW).

References

1. Schlögl, R. Heterogeneous catalysis. *Chem. Int. Ed.* **54**, 3465–3520 (2015).
2. Zheng, R. Y., Liu, Z. C., Wang, Y. D. & Xie, Z. K. Industrial catalysis: strategies to enhance selectivity. *J. Catal.* **41**, 1032–1038 (2020).
3. Tamura, M., Tokonami, K., Nakagawa, Y. & Tomishige, K. Selective hydrogenation of crotonaldehyde to crotyl alcohol over metal oxide modified ir catalysts and mechanistic insight. *ACS Catal.* **6**, 3600–3609 (2016).
4. Lan, X. C. & Wang, T. F. Highly selective catalysts for the hydrogenation of unsaturated aldehydes: a review. *ACS Catal*. **10**, 2764–2790 (2020).
5. Wu, B. H., Huang, H. Q., Yang, J., Zheng, N. F. & Fu, G. Selective hydrogenation of *α,β*-unsaturated aldehydes catalyzed by amine-capped platinum-cobalt nanocrystals. *Chem. Int. Ed.* **51**, 3440–3443 (2012).
6. Schoenbaum, C. A., Schwartz, D. K. & Medlin, J. W. Controlling the surface environment of heterogeneous catalysts using self-assembled monolayers. *Chem. Res.* **47**, 1438–1445 (2014).
7. Cano, I., Chapman, A. M., Urakawa, A. & van Leeuwen, P. W. N. M. Air-stable gold nanoparticles ligated by secondary phosphine oxides for the chemoselective hydrogenation of aldehydes: crucial role of the ligand. *Am. Chem. Soc*. **136**, 2520–2528 (2014).
8. Bai, S. X., Bu, L. Z., Shao, Q., Zhu, X. & Huang, X. Q. Multicomponent Pt-based zigzag nanowires as selectivity controllers for selective hydrogenation reactions. *Am. Chem. Soc.* **140**, 8384–8387 (2018).
9. Zhao, M. T., Yuan, K., Wang, Y., Li, G. D., Guo, J., Gu, L., Hu, W. P., Zhao, H. J. & Tang, Z. Y. Metal–organic frameworks as selectivity regulators for hydrogenation reactions. *Nature* **539**, 76–80 (2016).
10. Kennedy, G., Baker, L. R. & Somorjai, G. A. Selective amplification of C=O bond hydrogenation on Pt/TiO_2: catalytic reaction and sum-frequency generation vibrational spectroscopy studies of crotonaldehyde hydrogenation. *Chem. Int. Ed.* **53**, 3405–3408 (2014).
11. Wu, Q. F., Zhang, C., Arai, M., Zhang, B., Shi, R. H., Wu, P. X., Wang, Z. Q., Liu, Q., Liu, K., Lin, W. W., Cheng, H. Y. & Zhao, F. Y. A Pt/TiH_2 catalyst for ionic hydrogenation via stored hydrides in the presence of gaseous H_2. *ACS Catal*. **9**, 6425–6434 (2019).
12. Wang, X. F., Liang, X. H., Geng, P. & Li, Q. B. Recent advances in selective hydrogenation of cinnamaldehyde over supported metal-based catalysts. *ACS Catal*. **10**, 2395–2412 (2020).
13. Yang, Y. S., Rao, D. M., Chen, Y. D., Dong, S. Y., Wang, B., Zhang, X. & Wei, M. Selective hydrogenation of cinnamaldehyde over Co-based intermetallic compounds derived from layered double hydroxides. *ACS Catal.* **8**, 11749–11760 (2018).
14. Dai, Y. H., Gao, X., Chu, X. F., Jiang, C. Y., Yao, Y., Guo, Z., Zhou, C. M., Wang, C., Wang, H. M. & Yang, Y. H. On the role of water in selective hydrogenation of cinnamaldehyde to cinnamyl alcohol on PtFe catalysts. *Catal*. **364**, 192–203 (2018).
15. Ye, T. N., Li, J., Kitano, M., Sasase, M. & Hosono, H. Electronic interactions between a stable electride and a nano-alloy control the chemoselective reduction reaction. *Sci.* **7**, 5969–5975 (2016).

16. Fujita, S. I., Sano, Y., Bhanage, B. M. & Arai, M. Supported liquid-phase catalysts containing ruthenium complexes for selective hydrogenation of *α,β*-unsaturated aldehyde: importance of interfaces between liquid film, solvent, and support for the control of product selectivity. *Catal*. **225**, 95–104 (2004).
17. Piradashvili, K., Alexandrino, E. M., Wurm, F. R. & Landfester, K. Reactions and polymerizations at the liquid-liquid interface. *Rev.* **116**, 2141–2169 (2016).
18. Benjamin, I. Reaction dynamics at liquid interfaces. *Rev. Phys. Chem*. **66**, 165–188 (2015).
19. Agmon, N., Bakker, H. J.,Campen, R. K.,Henchman, R. H.,Pohl, P.,Roke, S., Thamer, & Ali Hassanali. A.Protons and hydroxide ions in aqueous systems. *Chem. Rev.* **116**, 7642–7672 (2016).
20. Zhao, G. L., Li, Y., Hong, B., Han, X., Zhao, S. L., Pera-Titus, M. & Liu, H. L. Nanomixing effects in glycerol/dodecanol Pickering emulsions for interfacial catalysis. *Langmuir* **34**, 15587–15592 (2018).
21. Bain, R. M., Pulliam, C. J., Thery, F. & Cooks, R. G. Accelerated chemical reactions and organic synthesis in leidenfrost droplets. *Chem. Int. Ed.* **55**, 10478–10482 (2016).
22. Dong, N., Zhang, Z. P., Xue, X. S., Li, X. & Cheng, J. P. Phosphoric acid catalyzed asymmetric 1,6-conjugate addition of thioacetic acid to para-quinone methides. *Chem. Int. Ed*. **55**, 1460–1464 (2016).
23. Zhang, B. Y., Jiang, Z. X., Zhou, X., Lu, S. M., Li, J., Liu, Y. & Li, C. The synthesis of chiral isotetronic acids with amphiphilic imidazole/pyrrolidine catalysts assembled in oil-in-water emulsion droplets. *Chem. Int. Ed.* **51**, 13159–13162 (2012).
24. Crossley, S., Faria, J., Shen, M. D. & Resasco, D. E. Solid nanoparticles that catalyze biofuel upgrade reactions at the water/oil interface. *Science* **327**, 68–72 (2010).
25. Shi, J. F., Wang, X. L., Zhang, S. H., Tang, L. & Jiang, Z. Y. Enzyme-conjugated ZIF-8 particles as efficient and stable Pickering interfacial biocatalysts for biphasic biocatalysis. *Mater. Chem. B* **4**, 2654–2661 (2016).
26. Song, Y., Michaels, T. C. T., Ma, Q. M., Liu, Z., Yuan, H., Takayama, S., Knowles, T. P. J. & Shum, H. C. Budding-like division of all-aqueous emulsion droplets modulated by networks of protein nanofibrils. *Commun.* **9**, 2110 (2018).
27. Pera-Titus, M., Leclercq, L., Clacens, J. M., De Campo, F. & Nardello-Rataj, V. Pickering interfacial catalysis for biphasic systems: from emulsion design to green reactions. *Chem. Int. Ed.* **54**, 2006–2021 (2015).
28. Wang, Z. P., van Oers, M. C., Rutjes, F. P. J. T. & van Hest, J. C. Polymersome colloidosomes for enzyme catalysis in a biphasic system. *Chem. Int. Ed*. **51**, 10746–10750 (2012).
29. Chen, Z. W., Zhou, L., Bing, W., Zhang, Z. J., Li, Z. H., Ren, J. S. & Qu, X. G. Light controlled reversible inversion of nanophosphor-stabilized Pickering emulsions for biphasic enantioselective biocatalysis. *Am. Chem. Soc.* **136**, 7498–7504 (2014).
30. Shan, Y. Y., Yu, C., Yang, J., Dong, Q., Fan, X. M. & Qiu, J. S. Thermodynamics-stability Pickering emulsion configured with carbon nanotubes-bridged nanosheet-shaped layered double hydroxide for selective oxidation of benzyl alcohol. *ACS Appl. Mater. Interfaces* **7**, 12203–12209 (2015).

31. Sun, Z. Y., Glebe, U., Charan, H., Böker, A. & Wu, C. Z. Enzyme-polymer conjugates as robust Pickering interfacial biocatalysts for efficient biotransformation ade reactions. *Chem. Int. Ed.* **57**, 13810–13814 (2018).
32. Potier, J., Menuel, S., Monflier, E. & Hapiot, F. Synergetic effect of randomly methylated *β* cyclodextrin and a dupramolecular hydrogel in Rh-catalyzed hydroformylation of higher olefins. *ACS Catal.* **4**, 2342–2346 (2014).
33. Gobbo, P., Patil, A. J., Li, M., Harniman, R., Briscoe, W. H. & Mann, S. Programmed assembly of synthetic protocells into thermoresponsive prototissues. *Nature Mater.* **17**, 1145–1153 (2018).
34. Jiang, H., Liu, L. D., Li, Y. X., Yin, S. W. & Ngai, T. Inverse Pickering emulsion stabilized by binary particles with contrasting characteristics and functionality for interfacial biocatalysis. *ACS Appl. Mater. Interfaces* **12**, 4989–4997 (2020).
35. Liu, C. C., Zhang, J. L., Zheng, L. R., Zhang, J., Sang, X. X., Kang, X. C., Zhang, B. X., Luo, T., Tan, X. N. & Han, B. X. Metal–organic framework for emulsifying carbon dioxide and water. *Chem. Int. Ed.* **55**, 11372–11376 (2016).
36. Zhou, W. J., Fang, L., Fan, Z. Y., Albela, B., Laurent Bonneviot, L., Campo, F. D., Pera-Titus, M. & Clacens, J. M. Tunable catalysts for solvent-free biphasic systems: Pickering interfacial catalysts over amphiphilic silica nanoparticles. *Am. Chem. Soc.* **136**, 4869–4872 (2014).
37. Faria, J., Ruiz, M. P. & Resasco, D. E. Phase-selective catalysis in emulsions stabilized by janus silica-nanoparticles. *Synth. Catal.* **352**, 2359–2364 (2010).
38. Chen, Z. J., Guan, Z. H., Li, M. R., Yang, Q. H. & Li, C. Enhancement of the performance of a platinum nanocatalyst confined within carbon nanotubes for asymmetric hydrogenation. *Chem. Int. Ed.* **50**, 4913–4917 (2011).
39. Liu, J., He, S., Li, C. M., Wang, F., Wei, M., Evans, D. G. & Duan, X. Confined synthesis of ultrafine Ru–B amorphous alloy and its catalytic behavior toward selective hydrogenation of benzene. *Mater. Chem. A* **2**, 7570–7577 (2014).
40. Narayan, S., Muldoon, J., Finn, M. G., Fokin, V. V., Kolb, H. C. & Sharpless, K. B., “On Water”: unique reactivity of organic compounds in aqueous suspension. *Chem. Int. Ed.* **44**, 3275–3279 (2005).
41. Song, C. E., Park, S. J., Hwang, I. S., Jung, M. J., Shim, S. Y., Han Yong Bae, H. Y. & Jung, J. Y. Hydrophobic chirality amplification in confined water cages. *Commun.* **10**, 851 (2019).
42. Jung, Y. & Marcus, R. A., On the theory of organic catalysis “on water”. *Am. Chem. Soc.* **129**, 5492–5502 (2007).
43. Hibbitts, D. D., Loveless, B. T., Neurock, M. & Iglesia, E. Mechanistic role of water on the rate and selectivity of Fischer–Tropsch synthesis on ruthenium catalysts. *Chem. Int. Ed.* **52**, 12273–12278 (2013).
44. Zhao, Z., Bababrik, R., Xue, W. H., Li, Y. P., Briggs, N. M., Nguyen1, D. T., Nguyen, U., Crossley, S. P., Wang, S. W., Wang, B. & Resasco, D. E. Solvent-mediated charge separation drives alternative hydrogenation path of furanics in liquid water. *Catal.* **2**, 431–436 (2019).

45. Li, G. N., Wang, B. & Resasco, D. E. Water-mediated heterogeneously catalyzed reactions. *ACS Catal.* **10**, 1294–1309 (2020).
46. Michel, C. & Gallezot, P. Why is ruthenium an efficient catalyst for the aqueous-phase hydrogenation of biosourced carbonyl compounds? *ACS Catal.* **5**, 4130–4132 (2015).
47. Zhang, K. L., Yang, Y. P., Liu, H., Liu, Q. X., Lv, J. L. & Zhou, H. F. Enantioselective synthesis of 2-hydroxyalkyl diarylphosphinates by Ruthenium-catalyzed asymmetric transfer hydrogenation. *Synth. Catal.* **361**, 4106–4110 (2019).
48. Bai, L., Greca, L. G., Xiang, W. C., Lehtonen, J., Huan, S. Q., Nugroho, R. W. N., Tardy, B. L. & Rojas, O. J. Adsorption and assembly of cellulosic and lignin colloids at oil/water interfaces. *Langmuir* **35**, 571–588 (2019).
49. Kalashnikova, I., Bizot, H., Bertoncini, P., Cathala, B. & Capron, I. Cellulosic nanorods of various aspect ratios for oil in water Pickering emulsions. *Soft Matter* **9**, 952–959 (2013).
50. Greydanus, B., Schwartz, D. K. & Medlin, J. W. Controlling catalyst-phase selectivity in complex mixtures with amphiphilic janus particles. *ACS Appl. Mater. Interfaces* **12**, 2338–2345 (2020).
51. Bradley, L. C., Stebe, K. J. & Lee, D. Clickable Janus Particles. *Am. Chem. Soc.* **138**, 11437–11440 (2016).
52. Zhang, M. J., Tang, Z. Y., Fu, W. Q., Wang, W. Y., Tan, R. & Yin, D. H. An ionic liquid-functionalized amphiphilic janus material as a Pickering interfacial catalyst for asymmetric sulfoxidation in water. *Commun.* **55**, 592–595 (2019).
53. Liang, F. X., Liu, B., Cao, Z. & Yang, Z. Z. Janus colloids toward interfacial engineering. *Langmuir* **34**, 4123–4131 (2018).
54. Bourikas, K., Stylidi, M., Kondarides, D. I. & Verykios, X. E. Adsorption of acid orange 7 on the surface of titanium dioxide. *Langmuir* **21**, 9222–9230 (2005).
55. Feng, T., Hoagland, D. A. & Russell, T. P. Assembly of acid-functionalized single-walled carbon nanotubes at oil/water interfaces. *Langmuir* **30**, 1072–1079 (2014).
56. Chaudhari, R. V., Bhanage, B. M., Deshpande, R. M. & Delmas, H. Enhancement of interfacial catalysis in a biphasic system using catalyst-binding ligands. *Nature* **373**, 501–503 (1995).
57. Sieffert, N. & Wipff, G. Importance of interfacial adsorption in the biphasic hydroformylation of higher olefins promoted by cyclodextrins: a molecular dynamics study at the decene/water interface. *Eur. J.* **13**, 1978–1990 (2007).
58. M. & Cordeiro. M. N. D. S. Intrinsic structure and dynamics of the water/nitrobenzene interface. *J. Phys. Chem. C* **111**, 17612–17626 (2007).
59. Lee, J. K., Samanta, D., Nam, H. G. & Zare. R. N. Micrometer-sized water droplets induce spontaneous reduction. *Am. Chem. Soc.* **141**, 10585–10589 (2019).
60. Mishra, H., Enami, S., Nielsen, R. J., Stewart, L. A., Hoffmann, R., Goddard, W. A. III & Agustín J. Colussi, A. J.Brønsted basicity of the air–water interface. *Proc. Natl. Acad. Sci. U. S. A.* **109**, 18679–18683 (2012).

61. Kasuga, T., Hiramatsu, M., Hoson, A., Sekino, T. & Niihara, K. Titania nanotubes prepared by chemical processing. *Mater.* **11**, 1307–1311 (1999).

Figures

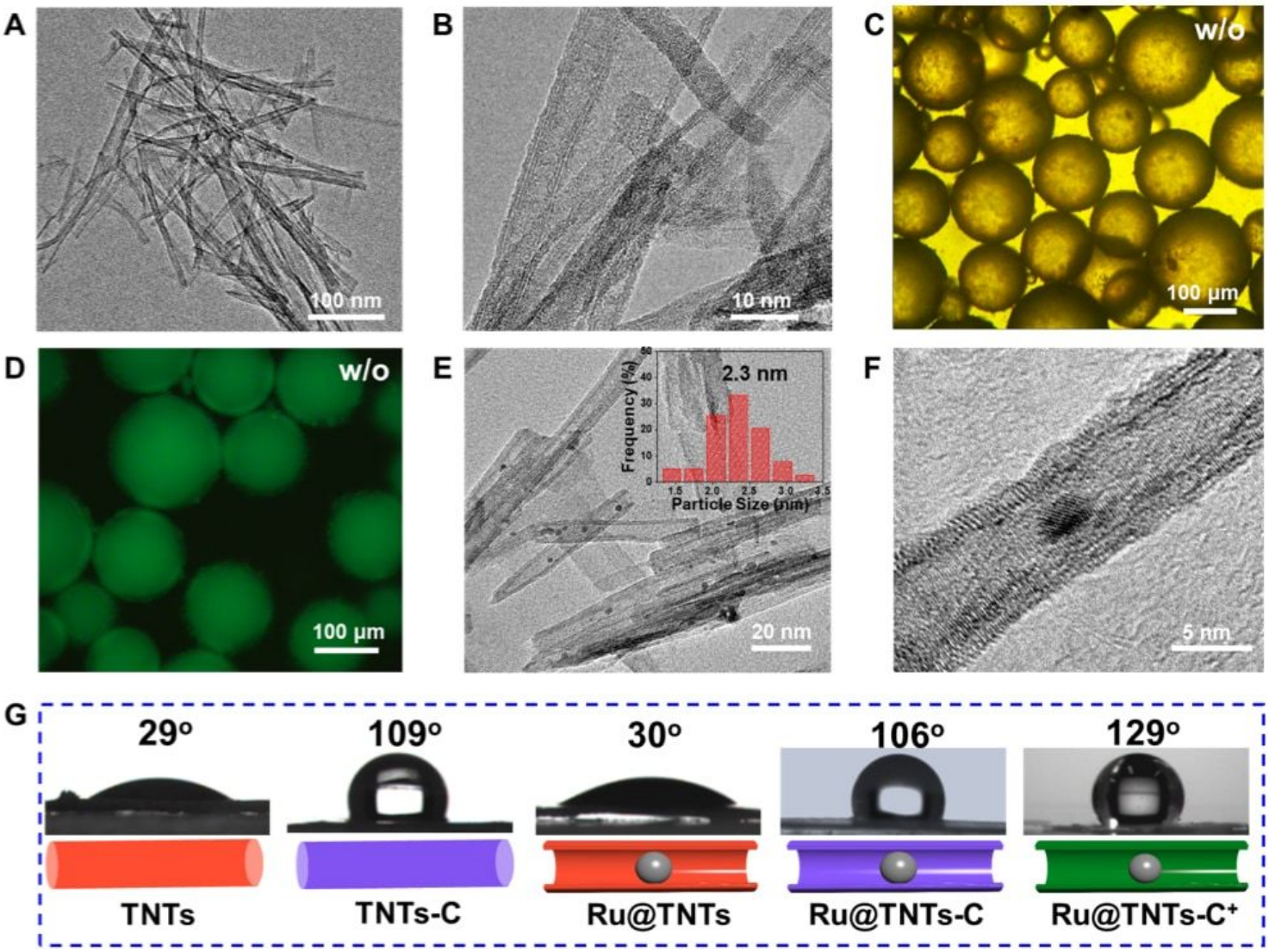

Figure 1

TEM images and water contact angles of different TNTs materials and micrographs of the w/o Pickering emulsion prepared with 2 wt.% TNTs-C (with respect to water). (A) TEM image of TNTs. (B) TEM image of TNTs-C. (C) Optical micrograph of the Pickering water-in-toluene emulsion. (D) Fluorescence confocal microscopy image of the Pickering emulsion with the water phase dyed by FITC-I. (E) TEM image of Ru@TNTs, inset showing Ru nanoparticle size distribution. (F) High magnification TEM image of the Ru@TNTs catalyst. (G) Water-air contact angles of various samples.

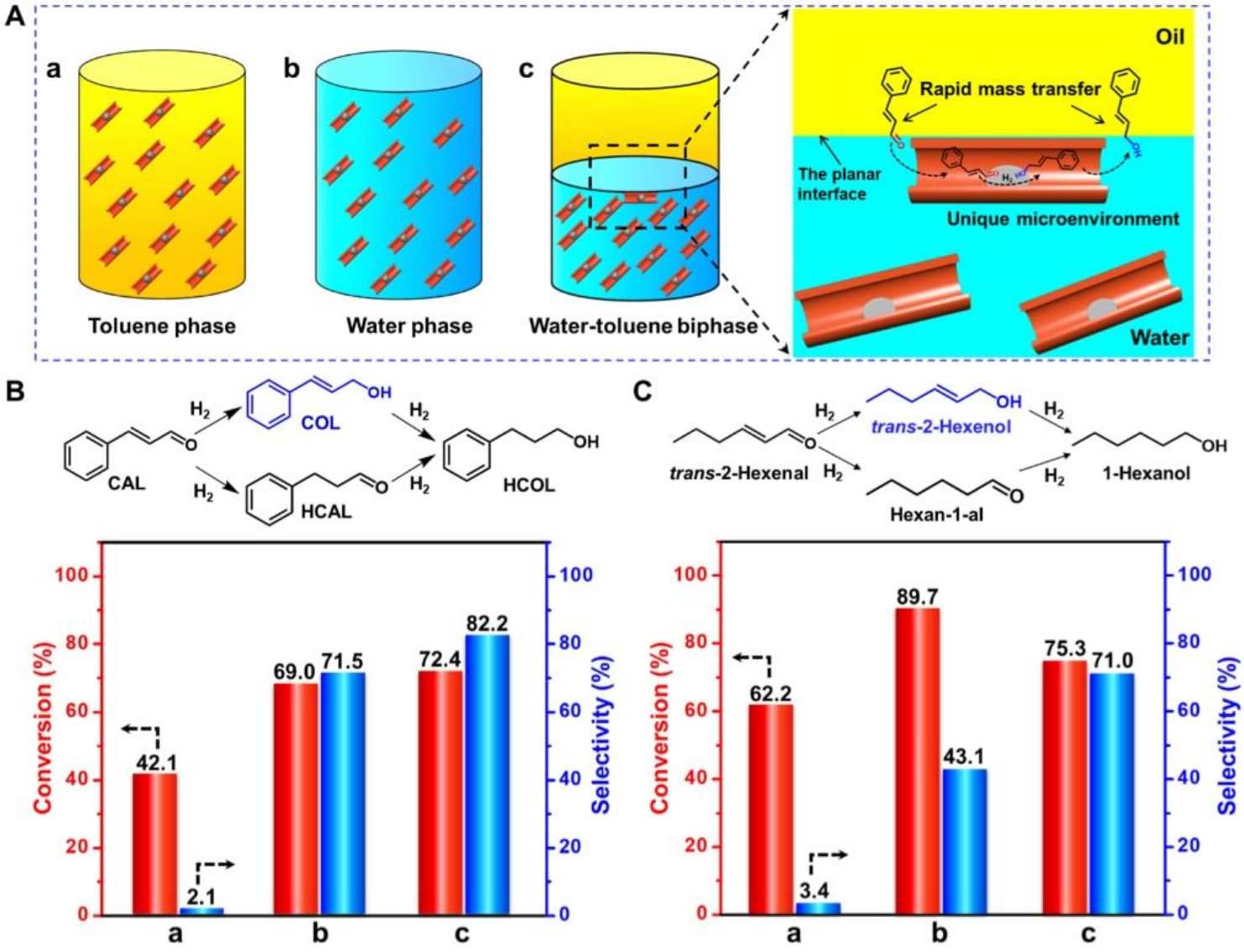

Figure 2

Conversion and selectivity of α,β-unsaturated aldehydes hydrogenation in different reaction systems. (A) Cartoon representing the different reaction systems: (a) single organic phase (5 mL toluene as solvent), (b) single aqueous phase (5 mL water as solvent), (c) water (2.5 mL)-toluene (2.5 mL) biphasic system and corresponding schematic illustration of the reaction taking place at the planar interface (TPPTS is omitted for clarification). Conversion and selectivity of (B) CAL and (C) trans-2-hexenal in different reaction systems. Reaction conditions: 0.05 g Ru@TNTs, 0.03 g TPPTS, 1.0 mmol CAL or trans-2-hexenal, 3.0 MPa H2, 60 oC, 700 rpm, 5 h.

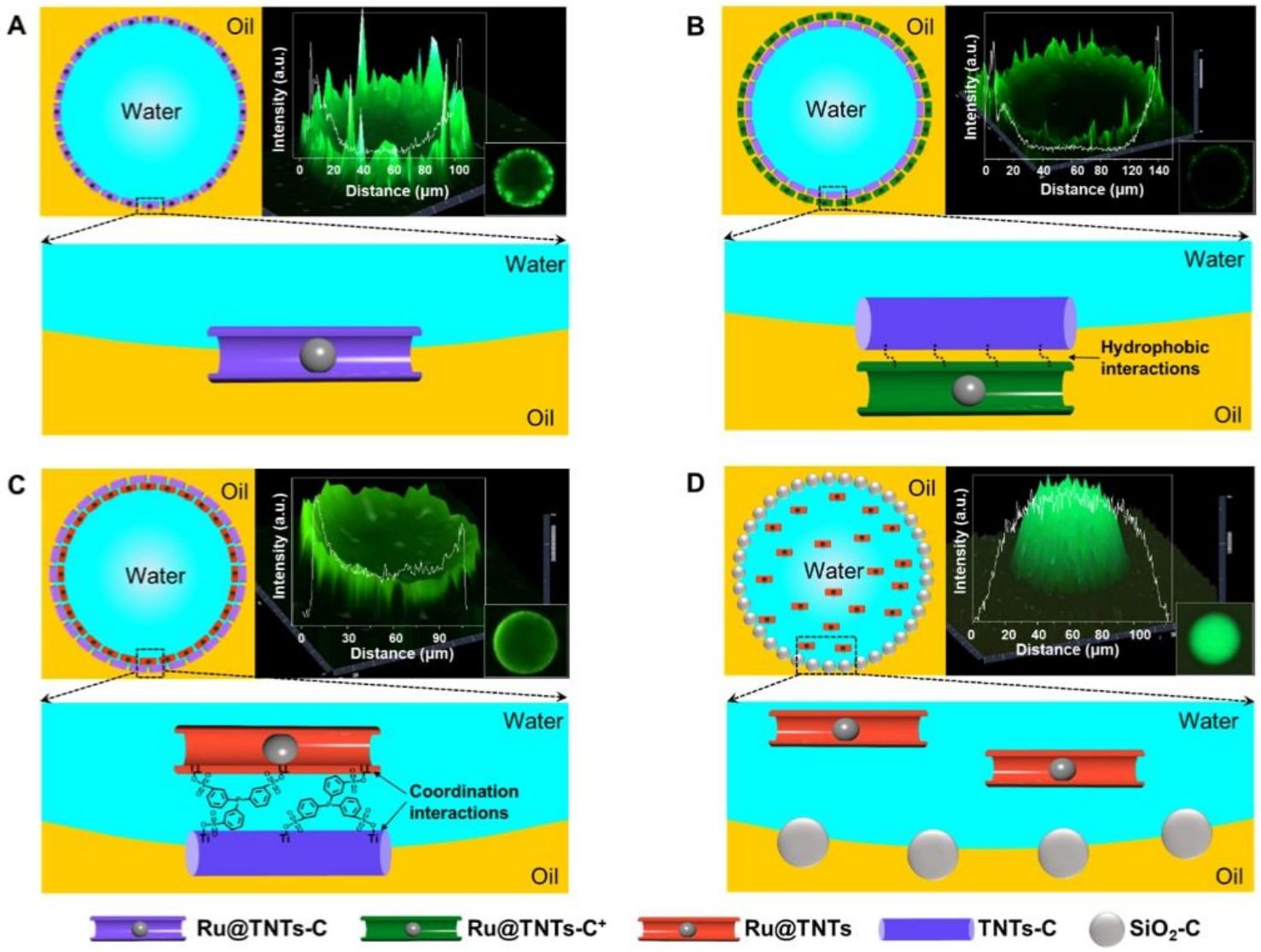

Figure 3

Cartoon depicting the catalyst locations within w/o Pickering emulsions and corresponding 3D fluorescence confocal micrographs. (A) Catalyst is located at the conventionally-called Pickering emulsion interface. (B) Catalyst is located at the outer interfacial layer of water droplets. (C) Catalyst is located at the inner interfacial layer of water droplets by the interaction of Ru@TNTs with TNTs-C. (D) Catalyst is distributed in the interior of droplets. The emulsion consists of 2.5 mL toluene, 2.5 mL water, 0.05 g FITC-I-labelled Ru@TNTs-C (for A), 0.05 g FITC-I-labelled Ru@TNTs-C+ (for B), 0.05 g FITC-I-labelled Ru@TNTs (for C and D), 0.05 g TNTs-C (for B and C), 0.05 g SiO2-C (for D), 0.03 g TPPTS. Drawings are not to scale.

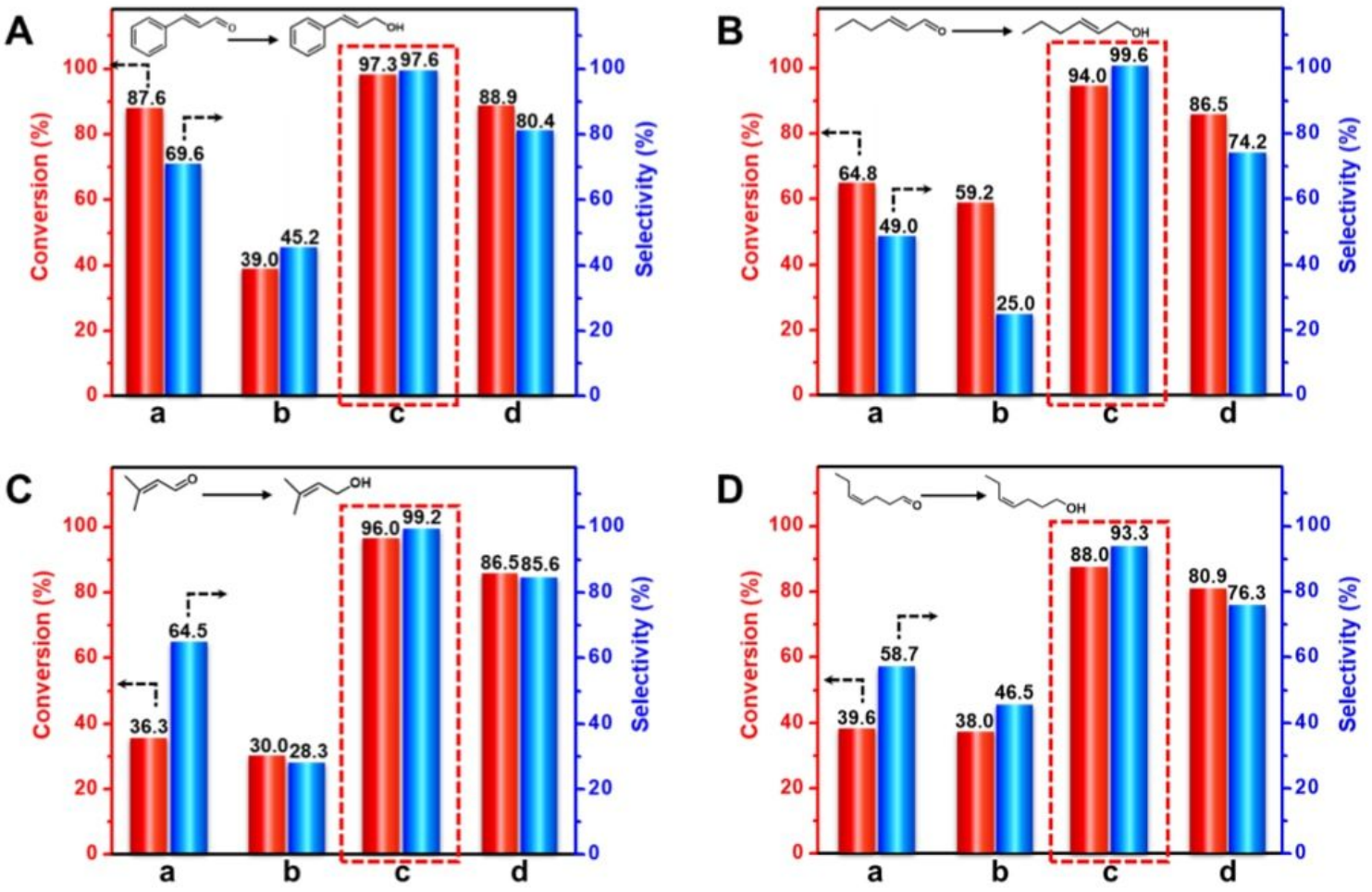

Figure 4

Results of unsaturated aldehydes hydrogenation in different reaction loci within w/o Pickering emulsions: (a) Catalyst is located at the conventionally-called Pickering emulsion interface, (b) catalyst is located at the outer interfacial layer of water droplets, (c) catalyst is located at the inner interfacial layer of water droplets, (d) catalyst is distributed in the interior of droplets. Conversion and selectivity for (A) CAL, (B) trans-2-hexenal, (C) 3-methyl-2-butenal, and (D) cis-4-heptenal hydrogenation in different reaction loci. Reaction conditions: 1.0 mmol unsaturated aldehydes, 2.5 mL toluene, 2.5 mL water, 0.05 g Ru@TNTs-C (for a), 0.05 g Ru@TNTs-C+ (for b), 0.05 g Ru@TNTs (for c and d), 0.05 g TNTs-C (for b and c), 0.05 g SiO2-C (for d), 0.03 g TPPTS, 60 oC, 3.0 MPa H2, 700 rpm, 5 h.

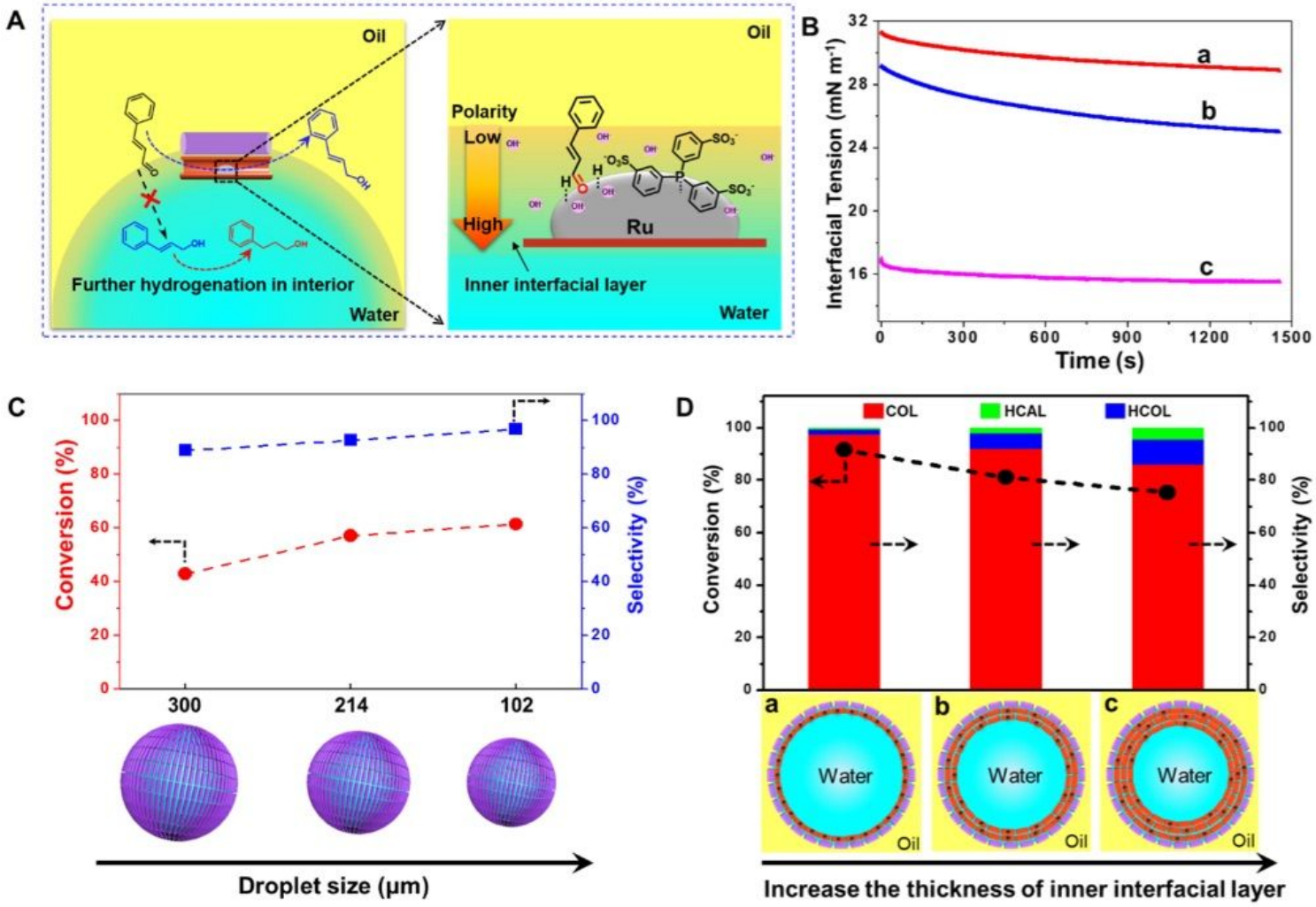

Figure 5

Proposed mechanism and evidence. (A) Schematic illustration of the inner interfacial layer reaction scenario. (B) Dynamic interfacial tensions in different water-toluene biphasic systems: (a) 3 mg mL-1 TPPTS in water, (b) 3 mg mL-1 TPPTS in water and 5 mg mL-1 TNTs-C in toluene, (c) 3 mg mL-1 TPPTS and 5 mg mL-1 TNTs in water, 5 mg mL-1 TNTs-C in toluene. (C) CAL conversion and COL selectivity versus droplet size in the inner interfacial layer reaction system, reaction time: 3 h. (D) CAL conversion and COL selectivity versus the thickness of inner interfacial layer in the inner interfacial layer reaction systems: (a) absence of TNTs, (b) adding 0.025 g TNTs, (c) adding 0.05 g TNTs. Other reaction conditions are same as those in Figure 4.

Supplementary Files

This is a list of supplementary files associated with this preprint. Click to download.

- SupplementaryInformationtoNatureCommunications.docx